Electrochimica Acta 414 (2022) 140210

Contents lists available at ScienceDirect

Electrochimica Acta

journal homepage: www.journals.elsevier.com/electrochimica-acta

Systematic study and effective improvement of voltammetry for accurate electrochemical window measurement of solid electrolytes

Zhenhan Fang [a,1], Zixin Hong [a,1], Yufeng Luo [c], Yang Liu [a], Hengcai Wu [a], Hui Tian [a], Fei Zhao [a], Yuegang Zhang [a,b], Qunqing Li [a,b], Shoushan Fan [a], Jiaping Wang [a,b,*]

[a] Department of Physics and Tsinghua-Foxconn Nanotechnology Research Center, Tsinghua University, Beijing 100084, China
[b] Frontier Science Center for Quantum Information, Beijing 100084, China
[c] Institute of Textiles and Clothing, Hong Kong Polytechnic University, Hong Kong, China

ARTICLE INFO

Keywords:
Lithium-ion battery
Solid electrolyte
Electrochemical window
Electric double layer
Step voltammetry

ABSTRACT

The availability of solid electrolytes promisingly boosts the energy density of lithium-ion batteries (LIBs), yet the accurate voltammetry measurement of their electrochemical windows (EWs) poses a longstanding and critical concern. In this work, the mechanism of EW measurement of electrolytes is explained using the electrical double layer theory. The influence of crucial variables in voltammetry, including the scan mode, the working electrode, and the selection of two- or three-electrode test systems is investigated. Furthermore, the step voltammetry method is proposed and applied to EW testing of the inorganic solid electrolyte $Li_{10}GeP_2S_{12}$ for the first time. Finally, suggestions for EW measurement of electrolytes are presented. The results of this work promote a comprehensive understanding and more accurate EW measurement of electrolytes, facilitating the selection of suitable solid electrolytes to match different cathodes, thus advancing the development of safer high-energy density LIBs.

1. Introduction

Lithium-ion batteries (LIBs) with high energy density, low self-discharge, and lightweight have become the main energy supply components for portable electronic devices in recent years [1]. However, with the development of large-scale energy storage devices such as electric vehicles, smart grids, and industrial energy storage, higher requirements for the energy density of LIBs have been put forward [2–4]. Two approaches are generally used to improve the energy density of LIBs. One is to further reduce the proportion of inactive substances in the battery by optimizing the battery preparation process. For example, energy density can be increased by reducing the mass of the current collector [5,6]. The other is to promote the performance of electrode materials, using active materials with higher capacity or higher operating voltage, such as sulfur [7], oxygen [8], silicon [9], and lithium metal [10].

Lithium metal is considered the most attractive negative electrode for high energy density LIBs with its high theoretical specific capacity (3860 mAh g^{-1}) and the lowest electrode potential (−3.04 V vs. standard hydrogen electrode). However, due to inhomogeneous lithium metal deposition, it is difficult to avoid the growth of lithium dendrites in the lithium negative electrode during cycling [11,12], which might lead to short circuits and even more severe safety issues such as thermal runaway [13,14]. A widely researched approach to improving the safety of lithium metal batteries is to substitute the traditional flammable liquid electrolyte with a solid electrolyte [15–17]. There are mainly three types of solid electrolytes: polymer electrolytes, inorganic electrolytes, and composite electrolytes [18]. Compared with liquid electrolytes, solid electrolytes possess the following advantages: (i) Solid electrolytes are non-volatile, non-leaking, and generally non-flammable, and can prevent LIBs from burning and exploding, thus leading to higher safety [19]. (ii) With the use of inorganic solid electrolytes with high Young's modulus, lithium metal can be safely adopted as the negative electrode, thus effectively promoting the energy density of LIBs [18,20,21]. (iii) Some inorganic solid electrolytes have much lower activation energy for ion migration, allowing solid batteries to operate over a wide temperature range (−50 to 200 °C) [19]. A pouch battery with a sulfide solid electrolyte and lithium negative electrode achieved an energy

* Corresponding author at: Department of Physics and Tsinghua-Foxconn Nanotechnology Research Center, Tsinghua University, Beijing 100084, China.
E-mail address: jpwang@tsinghua.edu.cn (J. Wang).
[1] These authors contributed equally to this work.

https://doi.org/10.1016/j.electacta.2022.140210
Received 5 December 2021; Received in revised form 28 February 2022; Accepted 10 March 2022
Available online 12 March 2022

density of more than 900 Wh L^{-1}, a stable coulombic efficiency of 99.8%, and a long life of 1000 cycles, showing a promising future of solid-state batteries [22].

Regardless of the above-mentioned advantages of solid electrolytes, there are still the following issues that need to be addressed to replace liquid electrolytes: (i) The interfacial problems between electrolyte and electrode needs to be solved [23]. Liquid electrolytes can effectively wet and infiltrate the gap on the electrodes. However, solid electrolytes (especially inorganic solid electrolytes), have inferior point contact with the electrode, resulting in a large contact resistance [24]. In addition, lithium dendrites remain inevitable with solid electrolytes, and the lithium metal negative electrode, especially defects, cracks, grain boundaries, and micro/nano-scale voids in the solid electrolytes, can induce faster growth of lithium dendrites [25]. (ii) The ionic conductivity of solid electrolytes needs to be enhanced. Some sulfide solid electrolytes have ionic conductivities comparable to those of liquid electrolytes at room temperature. For example, $Li_{10}GeP_2S_{12}$ (LGPS) has an ionic conductivity of 10^{-2} S cm^{-1} at 50–80 ℃ [26]. However, the room temperature ionic conductivities of most solid electrolytes, especially polymer electrolytes, still need to be improved. For instance, polyethylene oxide (PEO) has ionic conductivities of only 10^{-4} S cm^{-1} and 10^{-6} S cm^{-1} at 80 ℃ and room temperature, respectively [27]. (iii) Electrochemical windows (EWs) of electrolytes need to be widened. The EW of an electrolyte is the difference between its oxidation and reduction potentials, which represents the range of electrochemical potentials for stable operation of the electrolyte. Electrolytes with wide EWs can be utilized in LIBs with the lithium metal negative electrode and high-voltage positive electrode [28,29]. Accurate determination and widening of the EWs of electrolytes are essential to increase the energy density of LIBs.

In the literature, EW test results of solid electrolytes by voltammetry methods tend to be inaccurate [30–32]. For example, cyclic voltammetry (CV) results showed that $Li_7La_3Zr_2O_{12}$ (LLZO) was stable within the voltage range 0–8 V [33], but computational [31,34] and experimental [30] works revealed that LLZO decomposed at a voltage much less than 8 V. Lithium phosphorus oxynitride (LiPON) had a stable EW of 0–5.5 V as measured by linear sweep voltammetry (LSV) [34], but Brecht Put et al. found that LiPON decomposed at 4.3 V [35]. LGPS was first discovered by Kamaya et al. and its EW was measured to be 0–5 V by CV [26]. However, many computational and experimental works in recent years argued that LGPS had a much narrower EW [30,36–39]. Yongyao Xia et al. measured the oxidation potential of PEO at 5 V by CV using stainless steel (SS) working electrode, while PEO decomposed at 3.8 V using a carbon working electrode [40]. Cross-linked polyethylene glycol-based resin prepared in our previous work, had an oxidation potential of 4.8 V measured by LSV, but the infrared measurement demonstrated that the electrolyte decomposed at 4.4 V [41]. These studies reveal that EW measurement of solid electrolytes by voltammetry methods is not standard, and the use of different scan modes or working electrodes often yields different results, which hinders the development of solid electrolytes.

Herein, the mechanism of EW measurement by voltammetry methods is explained using the electric double layer (EDL) theory. The effects of scan mode, working electrode, and two- or three-electrode test system on the results are investigated, and the step voltammetry (SV) method is applied to EW testing of solid electrolyte LGPS for the first time. This work presents a thorough understanding of EW measurement of electrolytes by voltammetry methods, which facilitates the appropriate selection of electrolytes and significantly boosts the research of LIBs with higher energy density and better safety.

2. Experimental section

2.1. Fabrication of SS, rSS, and SS@C working electrodes

Working electrodes with different compositions and specific surface areas were prepared. SS electrodes were manufactured with a diameter of 10 mm and a thickness of 0.5 mm, and the rough SS (rSS) electrodes were obtained by rubbing the SS surface with abrasive paper. Carbon-coated SS (SS@C) electrodes were achieved by chemical vapor deposition on SS surface with acetylene precursor.

2.2. Fabrication of CNT and CNT/AC working electrodes

60 mg super-aligned carbon nanotubes (SACNTs) [42] were added to 80 ml ethanol and sonicated for 30 min to produce a homogeneous dispersion. A flexible and self-supporting CNT film was obtained by vacuum filtration, which was then cut into discs with a diameter of 10 mm for use as the CNT working electrodes. CNT/activated carbon (CNT/AC) working electrodes were prepared in the same way, except that 60 mg SACNTs and 60 mg AC powder were used together for dispersion in ethanol.

2.3. Assembly of two-electrode and three-electrode cells

Two-electrode cells were assembled in an argon glove box (M. Braun Inset Gas Systems Co., Ltd., Germany) with CR-2016 shell, SS, rSS, SS@C, CNT, or CNT/AC working electrode, lithium (China Energy Lithium Co., Ltd.) counter electrode, and liquid electrolyte that was prepared by dispersing 1 M lithium hexafluorophosphate ($LiPF_6$) in a mixture of ethylene carbonate (EC) and dimethyl carbonate (DMC) (1:1 vol%). For the cells with solid electrolyte, a two-electrode mold (Hefei Kejing Materials Technology Co., LTD) was employed to cold-press SS, CNT, or CNT/AC working electrode with 100 mg LGPS for 3 min, followed by the assembly with a 10 mm diameter lithium sheet. A two-electrode mold and SS, CNT, and CNT/AC symmetric cells were used to measure the ionic conductivity of the solid electrolyte LGPS. Three-electrode cells were assembled using a uniquely designed three-electrode mold with CNT as the working electrode, LGPS as the solid electrolyte, lithium sheet as the counter electrode, and lithium ring as the reference electrode. The counter electrode and the reference electrode were isolated by a polyether ether ketone (PEEK) insulating ring.

2.4. Material characterization

The frontal and cross-sectional morphologies of the SS, rSS, SS@C, CNT, and CNT/AC electrodes were characterized by scanning electron microscopy (SEM, Sirion 200, FEI, USA). The specific surface areas of the electrodes were obtained by BET measurements on a surface area and porosity analyzer (ASAP 2020). The PARSAT2273 (AMETEK) electrochemical workstation was used to measure LSV, CV (scan rate: 1 mV s^{-1}), and Tafel curves (scan rate: 0.1 mV s^{-1}) of electrolytes. The Vertex. C (IVIUM) electrochemical workstation was employed to conduct SV and ionic conductivity (frequency range: 100 kHz-0.1 Hz, AC amplitude: 30 mV) measurements of solid electrolytes, and the Land CT2001 automated battery tester was utilized to monitor the potential difference between the counter electrode and the reference electrode. All electrochemical tests were conducted at room temperature.

2.5. Finite element simulation

Electrochemical models were constructed using the electrochemical module of COMSOL Multiphysics 5.5. Based on the finite element solver, the cell potential distribution was calculated in equilibrium, reduction, and oxidation states.

3. Results and discussion

Voltammetry is the most commonly used method to measure the EW of electrolytes. Typically, lithium is used as the counter electrode, and SS, carbon, or other inert materials that cannot store lithium serves as the working electrode. Based on the location of the redox peaks, the

potentials at which the electrolyte undergoes redox reactions are determined. At present, EW measurement of electrolytes lacks an accurate and feasible standard. In particular, the selection of scan mode, working electrode, and two- or three-electrode system has not been systematically investigated. Therefore, this work aims to study the influence of these testing parameters on EW results and suggest suitable measurement methods, which provides a better way to investigate the inherent properties of electrolytes and explore their practical applications.

3.1. *Mechanism of voltammetry for measuring EW of electrolytes by the EDL theory*

Fig. 1a and 1b show schematics of typical current-voltage curves for EW measurement of reduction and oxidation potentials, respectively. During the cathodic scan (Fig. 1a), when the potential is gradually reduced from the open-circuit voltage, the current remains essentially constant at first and then forms a reduction peak. The reduction onset potential $V_{o\text{-reduction}}$ corresponds to the intersection of the current peak tangent with the initial current baseline, and the reduction peak potential is the voltage at the current peak. Similarly, when the oxidation potential is measured during the anodic scan (Fig. 1b), the oxidation onset potential $V_{o\text{-oxidation}}$ and the peak potential $V_{p\text{-oxidation}}$ can also be obtained from the current signal.

For the accurate measurement of the EW of electrolytes, it is important to determine whether V_p or V_o should be chosen as the redox potential. The interface between the working electrode and the electrolyte during the voltammetry measurement is considered. When two different objects are in contact, the particles at the interface and the internal particles are subjected to different forces, which yields an EDL structure [43,44]. A Stern EDL model is illustrated in Fig. 1c, where a compact layer and a diffuse layer are formed in the electrolyte under the combined effects of electrostatic interactions and thermal diffusion [45]. The potentials of the working electrode and the electrolyte in the compact layer are noted as Φ_W and Φ_E, respectively, and a potential difference $\Delta\Phi = \Phi_W - \Phi_E$ exists, which is defined as the electrode potential. Before the potential reaches the onset redox potential (corresponding to $V_{o\text{-reduction}}$ in Fig. 1a and $V_{o\text{-oxidation}}$ in Fig. 1b), the change of potential merely induces charging and discharging of the EDL, altering the interface structure and generating non-Faraday currents. When the potential reaches $V_{o\text{-reduction}}$ or $V_{o\text{-oxidation}}$, the electrolyte commences a redox reaction and charge transfer begins to take place at the interface, characterized by the onset of the current (i.e., the appearance of the Faraday current). As the potential exceeds the onset redox potential, ions in the compact layer are further consumed. The current signal attains a peak (i.e., $V_{p\text{-reduction}}$ in Fig. 1a and $V_{p\text{-oxidation}}$ in Fig. 1b) when there are not sufficient ions in the compact layer and ions in the diffuse layer have not yet spread to the interface. The onset potential originates from the emergence of Faraday currents and indicates the beginning of the redox reaction. Whereas, the peak potential is formed subject to factors such as thermal diffusion within the electrolyte after the redox reaction occurs. Therefore, it makes more sense to choose the onset potential as the redox potential of the electrolyte rather than the peak potential for EW measurement.

Experimental results have shown that there are deviations between the measured and true EW values of electrolytes (i.e., there is still a deviation between V_o and the actual redox potential of the electrolyte) [46]. An electrode polarization model is proposed to explain such phenomena. For the electrode in an electrolyte, when the redox state particles are in dynamic equilibrium without any net current, the

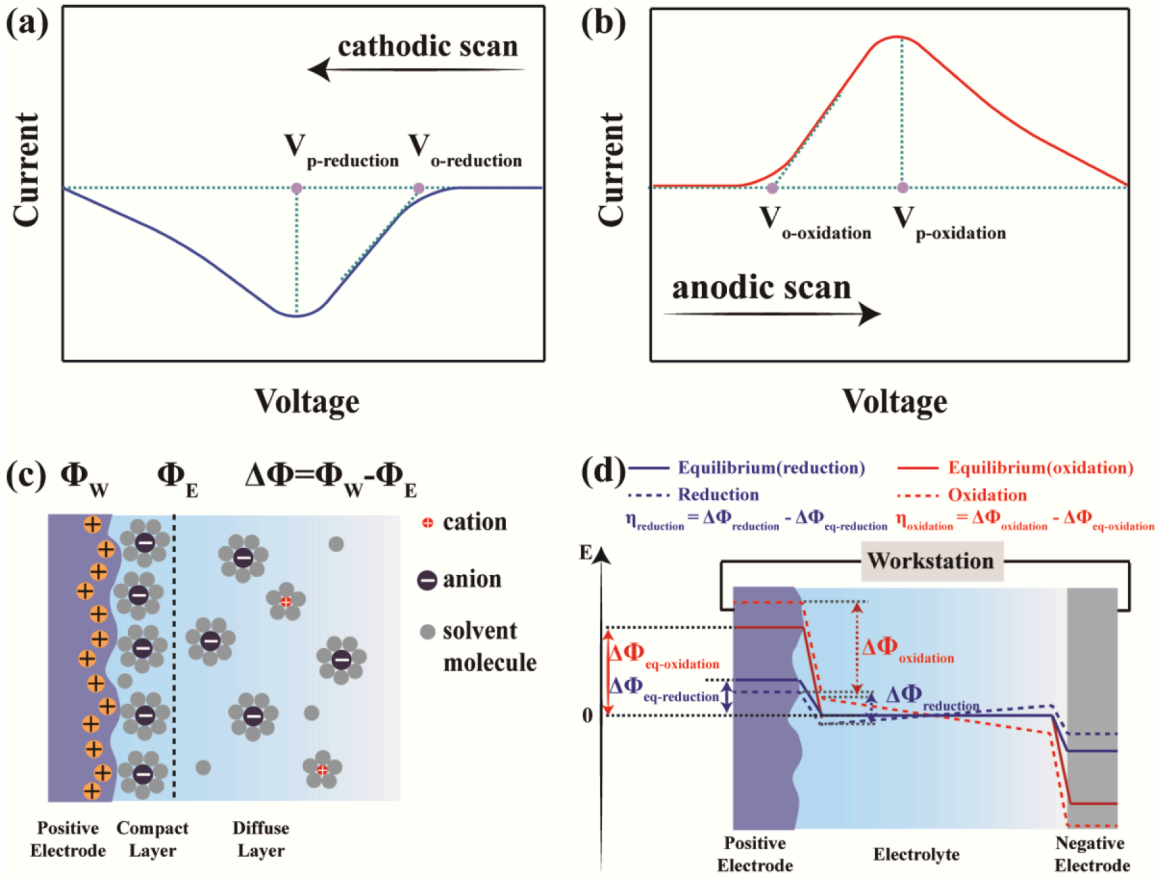

Fig. 1. The schematic of current-voltage curves for EW measurement of (a) reduction and (b) oxidation potentials. (c) Schematic diagram of the Stern EDL model. (d) Cell potential distribution in equilibrium, oxidation, and reduction states.

corresponding potential is called the equilibrium potential [47]. Ideally, the electrolyte should undergo redox reactions at the equilibrium potential for EW characterization. However, in the actual measurement, electrode polarization exists, where the electrode potential deviated from the equilibrium potential by an overpotential [43]. To some extent, the overpotential reflects the degree to which the measured EW differs from the true value. Finite element simulations of the cell potential distribution are shown in Fig. S1, where the electrode polarization causes the reduction potential lower than the equilibrium potential and the oxidation potential higher than the equilibrium potential. Fig. 1d shows the schematic of the cell potential distribution in equilibrium, oxidation, and reduction states. The blue/red solid lines indicate the cell potential distribution when the electrolyte is at the reduction/oxidation equilibrium potential, and the potential difference of the EDL is denoted as $\Delta\Phi_{eq\text{-}reduction}/\Delta\Phi_{eq\text{-}oxidation}$. When the actual reduction/oxidation reaction occurs, the electrode is polarized. The blue and red dashed lines illustrate the potential distribution, and the corresponding EDL potential differences are expressed as $\Delta\Phi_{reduction}$ and $\Delta\Phi_{oxidation}$. The oxidation overpotential $\eta_{oxidation}$ ($\Delta\Phi_{oxidation} - \Delta\Phi_{eq\text{-}oxidation}$) and reduction overpotential $\eta_{reduction}$ ($\Delta\Phi_{reduction} - \Delta\Phi_{eq\text{-}reduction}$) exist in practical measurement. Thus, the electrode polarization produces a redox overpotential, which causes the measured redox potential to deviate from the true value. The smaller the absolute value of the overpotential, the closer the measured redox potential to the true value. A detailed investigation of the overpotential and redox potential of electrolytes is conducted in this work.

3.2. Effect of scan mode on EW measurement of electrolytes

Among the voltammetry methods reported in the literature, LSV and CV scan modes are the most prevalent, in which a linearly varying potential is applied to the working electrode. For the LSV scan mode, the potential is unidirectional, whereas the CV scan mode features an additional reverse sweep back. When the scanning potential reaches the electrolyte redox potential, a redox reaction occurs in the electrolyte and the charge transfer between the electrolyte and the electrode takes place, generating a Faraday current. It was found in the literature that for the same working electrode and electrolyte, different redox potentials were obtained using LSV and CV scan modes [46]. To focus more on the effect of scan mode on EW measurements, a liquid electrolyte was chosen in this work to avoid the poor contact problem between solid electrolytes and electrodes.

Four scan modes were used to measure the redox potentials of the liquid electrolyte (Fig. S2): LSV scan from the open-circuit voltage V_{oc} to 7 V and from V_{oc} to 0 V (scan mode 1); LSV scan from 0 V to 7 V (scan mode 2); CV scan from V_{oc} to 0 V, 7 V, and then V_{oc} (scan mode 3); and CV scan from V_{oc} to 7 V, 0 V, and then V_{oc} (scan mode 4). $V_{o\text{-}reduction}$ values of 1.65 V, 1.65 V, and 2.07 V were obtained by scan modes 1, 3, and 4. $V_{o\text{-}reduction}$ could not be measured by scan mode 2. $V_{o\text{-}oxidation}$ results of 4.13 V, 4.55 V, 4.70 V, and 4.13 V were achieved by scan modes 1, 2, 3, and 4.

The discrepancy among the redox potential results using four scan modes can be explained by the interfacial reaction products. By scan mode 1, the electrolyte redox reaction occurs without the influence of solid electrolyte interlayer (SEI) or cathode electrolyte interlayer (CEI) at the electrolyte/electrode interface, and EW measurement is relatively accurate (Fig. S2a). By scan modes 2–4, the measured onset potentials are relatively accurate when the oxidation or reduction potential is first reached. However, as the potential deviates from the redox potential, the electrolyte involved in the reaction gradually increases. More amounts of SEI and CEI are generated, leading to additional redox peaks in subsequent tests, which affect the EW results. Therefore, to obtain a more accurate EW of the electrolyte, it is recommended to use scan mode 1, i.e., LSV scan starting from V_{oc} for both anodic and cathodic scans.

3.3. Effect of the working electrode on EW measurement of electrolytes

In addition to the scan mode, the use of various working electrodes also causes different EW results [48–51]. The role of the working electrode in the EW measurement process is investigated. At equilibrium potential, there is a dynamic equilibrium of charge transfer at the working electrode/electrolyte interface for both oxidation and reduction, and the electron flow results in an exchange current density j_0 [52]. Finite element simulations of the cell potential reveal that j_0 of the working electrode impacts the redox overpotential (Fig. 2a). The contact of different working electrodes with the electrolyte generates various exchange current densities, which alters the overpotential and further affects the redox potential. Simulation results in Fig. 2a exhibit a negative reduction overpotential. At higher j_0 of the working electrode, the absolute value of the reduction overpotential is smaller, and the measured $V_{o\text{-}reduction}$ is closer to the equilibrium reduction potential. A similar analysis applies to the measurement of the oxidation potential.

J_0 correlates with many factors, including the specific reaction, the concentration of the reacting substance, and material type and surface area of the electrode [45]. For the EW determination of an electrolyte with a given specific reaction and concentration of the reacting material, the effects of the surface area and material type of the working electrode on j_0 and EW were investigated. The most commonly available SS electrode was used for a comparative investigation. The rSS electrode had a larger surface area than the SS electrode. The SS@C electrode had the same surface area as the SS electrode and their material types were different. The SEM images of the surfaces and cross-sections of the electrodes demonstrate that the SS and SS@C electrodes had flat surfaces (Fig. 2d, e, g, h), while the rSS electrode exhibited a rough surface and a larger surface area (Fig. 2f, i). J_0 can be derived from the Tafel curve of the working electrode [53]. The j_0 of the SS, SS@C, and rSS electrodes were 8.39×10^{-8} A cm^{-2}, 1.13×10^{-7} A cm^{-2} and 2.17×10^{-7} A cm^{-2}, respectively (Fig. 2b). These results suggest that j_0 varied with both material type and surface area. For the same material type, j_0 increased with the increment of the surface area. With the same surface area, the use of carbon material led to a larger j_0 than SS.

SS, SS@C, and rSS electrodes were used to evaluate EW of the liquid electrolyte (Fig. 2c) to experimentally verify the simulation results in Fig. 2a, that is, a working electrode with a large j_0 leads to a small absolute value of the overpotential and a minor deviation of the redox potential from the equilibrium potential. The solid line in Fig. 2c refers to the measured data and the dashed line is the tangent to the current peak that is used to identify the onset potential. For the SS, SS@C, and rSS electrodes, the measured reduction onset potentials $V_{o\text{-}reduction}$ were 1.38 V, 1.55 V, and 1.72 V, and the measured oxidation onset potentials $V_{o\text{-}oxidation}$ were 4.13 V, 4.08 V, and 4.02 V, respectively. Table 1 summarizes the j_0 and onset redox potentials of the electrodes. The use of a working electrode with a larger j_0 (such as rSS) produced a higher $V_{o\text{-}reduction}$ and a smaller $V_{o\text{-}oxidation}$ that were closer to the true redox potentials. These results indicate that for a liquid electrolyte, a larger j_0 leads to a smaller absolute value of the overpotential, as well as a smaller deviation from the true redox potentials, which agrees well with the finite element simulation results in Fig. 2a.

Furthermore, the effect of the working electrode on EW measurement of solid electrolytes was investigated for the first time. Considering the poor contact between solid electrolyte and electrode, inert materials with higher surface area and better flexibility than rSS are required as working electrodes. Here, self-supporting and flexible CNT films that possessed a continuous conducting network structure [54] were used as the CNT working electrodes. Flexible CNT/AC working electrodes with an even higher specific surface area were also prepared (Fig. S3). The SS electrode with a smooth surface had poor point-to-point contact with the solid electrolyte LGPS (Figs. 3a, d and S4a), whereas the CNT and the CNT/AC electrodes were flexible (Fig. S4b–e) and provided better contact with LGPS (Fig. 3b, c, e, f). The Tafel curves in Fig. S5 show that the j_0 of SS, CNT, and CNT/AC electrodes were 8.39×10^{-8} A cm^{-2},

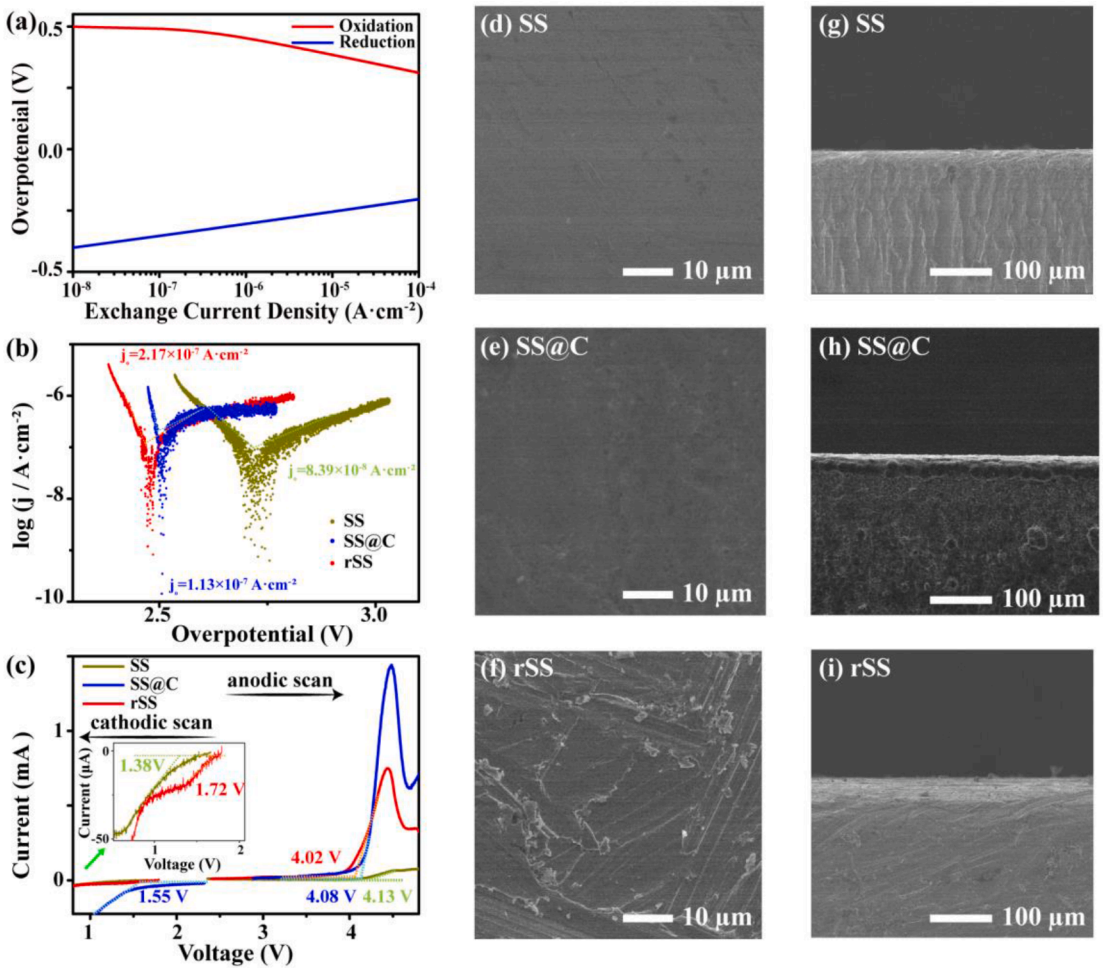

Fig. 2. (a) Relationship between redox overpotential and exchange current density. (b) Tafel curves and (c) EW measurement using the SS, SS@C, rSS electrodes. Surface and cross-sectional SEM images of the (d,g) SS, (e,h) SS@C, (f,i) rSS electrodes.

Table. 1
j_0, $V_{o\text{-reduction}}$, and $V_{o\text{-oxidation}}$ of the SS, SS@C, rSS working electrodes.

Materials	SS	SS@C	rSS
j_0 (A cm^{-2})	8.39×10^{-8}	1.13×10^{-7}	2.17×10^{-7}
$V_{o\text{-reduction}}$ (V)	1.38	1.55	1.72
$V_{o\text{-oxidation}}$ (V)	4.13	4.08	4.02

1.33×10^{-6} A cm^{-2}, and 4.64×10^{-6} A cm^{-2}, respectively. According to the characterization method of the kinetic parameters [55–58], the ionic conductivities of the LGPS were measured as 1.7×10^{-3} S cm^{-1}, 4.0×10^{-3} S cm^{-1}, and 4.2×10^{-3} S cm^{-1} using the SS, CNT, and CNT/AC electrodes, respectively (Fig. S6).

The onset reduction potentials $V_{o\text{-reduction}}$ of LGPS using SS, CNT, and CNT/AC electrodes were 1.10 V, 1.29 V, and 1.39 V (Fig. 3g). The $V_{o\text{-reduction}}$ rose with the increase of the j_0 of the working electrode. The onset oxidation potential $V_{o\text{-oxidation}}$ could not be measured using the SS electrode due to the poor contact between SS and LGPS (Fig. 3a). Using CNT and CNT/AC electrodes with better contact with LGPS, the $V_{o\text{-oxidation}}$ were 2.80 V and 2.76 V. The experimental redox potential results of solid electrolyte LGPS also agree well with the simulation results in Fig. 2, demonstrating that a higher j_0 induces a smaller absolute value of

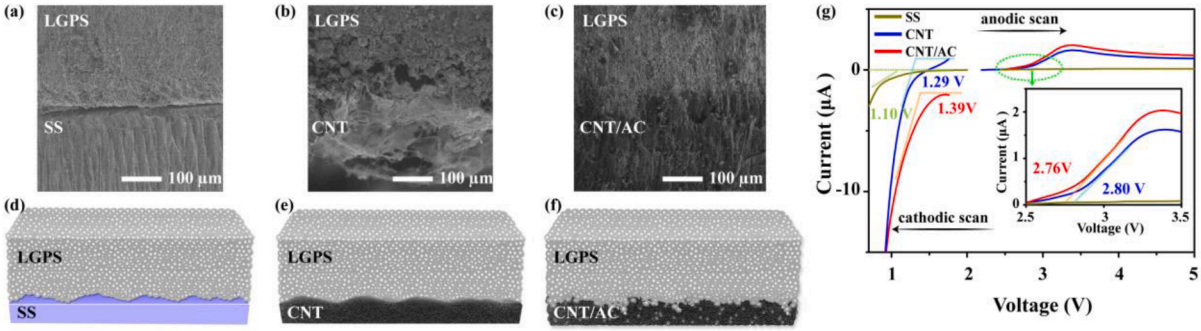

Fig. 3. SEM images and schematic diagrams of the contact interfaces between (a,d) SS, (b,e) CNT, (c,f) CNT/AC electrodes and LGPS. (g) EW measurement of LGPS using different working electrodes.

overpotential and a more accurate redox potential result. The redox potentials of a liquid electrode using the SS, CNT, and CNT/AC working electrodes (Fig. S7) confirm the conclusion. The measured onset redox potentials of the liquid electrolyte and solid electrolyte LGPS are listed in Table 2.

The limitations of using working electrodes with large surface areas and high j_0 were also observed. The large surface areas of the CNT and CNT/AC electrodes produced significant non-Faraday currents. Blue and red curves in Fig. 3g show that cells assembled with the CNT and CNT/AC electrodes had a non-zero initial potential before the peak formation during the cathodic scan, and the potential varied drastically. These make the baseline difficult to determine, leading to inaccurate measurement of the reduction potential. Such phenomena appeared similarly in the liquid electrolyte (Fig. S7). Therefore, the specific surface area of the working electrode should not be too high and the effect of non-Faraday current on the test results must also be considered for the determination of the redox potentials of electrolytes.

The above experimental results demonstrate that various materials and surface areas of the working electrodes offer distinct j_0, leading to different overpotentials and redox potentials. Working electrodes with higher surface areas generate remarkable non-Faraday currents that might mislead the redox potential determination (Figs. 3g and S7g). Therefore, it is advisable to adopt working electrodes with moderate surface area and high j_0, such as SS and CNT films. SS is cheap and readily available, and can be used to effectively determine the redox potential of liquid electrolytes, but is not suitable for EW measurements of solid electrolytes. Flexible porous CNT films can effectively provide good contact with solid electrolytes, but possess larger non-Faraday currents than SS. As a result, there is still a lack of superior working electrode candidates for EW measurement of solid-state electrolytes.

3.4. SV for EW measurement of solid electrolyte LGPS

The electron transfer kinetics for solid electrolytes was relatively slow because of the low conductivity and the poor contact at the interface between the SS electrode and the LGPS electrolyte. Therefore, it is unfeasible to measure the EW of solid electrolytes using conventional voltammetry methods. It is desirable to develop a modified voltammetry method for accurate EW measurement of solid electrolytes. In our previous work, the SV method was used to measure the EW of solid polymer electrolytes, which demonstrated high accuracy and short test times for materials with low electrical conductivity [41]. Here, the SV method was extended to EW measurement of inorganic solid electrolyte LGPS using SS working electrode. The SV method controls the process by adjusting the amount of each potential change ΔU and the relaxation time Δt [59]. A certain voltage U is applied and held for Δt. Then the voltage is changed to $U+\Delta U$ and kept for Δt, and so forth until the end. Relaxation time Δt is maintained after each voltage variation, which effectively improves the electron transfer dynamics of solid electrolytes.

ΔU was set as 0.02 V and Δt was set at 75 s, 150 s, and 300 s, respectively (Fig. 4). The $V_{o\text{-reduction}}$ results for Δt at 75 s, 150 s, and 300 s were 1.52 V, 1.55 V, and 1.55 V, higher than 1.10 V in Fig. 3g by the LSV method. The increased Δt permitted a longer time for electron transfer from SS to LGPS. When Δt was long enough to complete the electron transfer process, such as a relaxation time of 150 s, the measured redox potential became constant. The same procedure and mechanism were applied to the measurement of oxidation potential. The relaxation time of 75 s was not adequate for the electron transfer (Fig. 4d), while at Δt of 150 s and 300 s (Fig. 4e, f), the $V_{o\text{-oxidation}}$ was measured as 2.46 V.

To conclude, the $V_{o\text{-oxidation}}$ of LGPS could not be detected by conventional voltammetry (Fig. 3g), and its EW could not be determined. Whereas the $V_{o\text{-reduction}}$ and $V_{o\text{-oxidation}}$ of LGPS were 1.55 V and 2.46 V by the SV method, showing its EW of 1.55–2.46 V, which coincides with the 0–1.7 V reduction potential and 2–2.5 V oxidation potential of LGPS derived from first-principle calculations and experimental results in the literature [60]. The superior SV method can be used to measure the EW of other low-conductivity materials. The electron response rate can be effectively boosted by setting appropriate ΔU and Δt, and a more accurate and efficient EW acquisition method is developed while ensuring minimal non-Faraday currents.

Table. 2
j_0, redox onset potentials of liquid electrolyte and solid electrolyte LGPS using the SS, CNT, CNT/AC working electrodes.

Materials	SS	CNT	CNT/AC
j_0 (A cm^{-2})	8.39×10^{-8}	1.33×10^{-6}	4.64×10^{-6}
$V_{o\text{-reduction}}$ of liquid electrolyte (V)	1.38	1.98	2.65
$V_{o\text{-oxidation}}$ of liquid electrolyte (V)	4.13	4.04	3.53
$V_{o\text{-reduction}}$ of LGPS (V)	1.10	1.29	1.39
$V_{o\text{-oxidation}}$ of LGPS (V)	–	2.80	2.76

3.5. Selection of two- or three-electrode system for EW measurement of solid electrolytes

In the above-mentioned experiments, a two-electrode system was used for EW measurement of electrolytes, where a lithium foil served as both counter and reference electrode. Yet, the potential of lithium might change during testing and thus impact the EW measurement of electrolytes. In this section, EW measurements of solid electrolyte LGPS using two- and three-electrode systems are discussed. A three-electrode device was designed (Fig. 5a). To ensure good electrode/electrolyte contact, CNT film was used as the working electrode. The cathodic and anodic scans in Fig. 5b show that the $V_{o\text{-reduction}}$ results of LGPS were 1.29 V and 1.39 V using two- and three-electrode systems, respectively, and the $V_{o\text{-oxidation}}$ values were 2.80 V for both systems.

In the three-electrode system, the potential variations in the counter electrode were assessed by monitoring the difference between the counter electrode and the reference electrode (V_{RE}-V_{CE}, Fig. 5c, d). At the beginning of the cathodic scan, the potential of the counter electrode and the reference electrode were equivalent; afterward, the potential of the counter electrode became larger than that of the reference electrode; eventually, the counter electrode potential was 0.10 V higher than the reference electrode potential (Fig. 5c). In a two-electrode system, the $V_{o\text{-reduction}}$ is the potential difference between the working electrode and the counter electrode, while in a three-electrode system, the $V_{o\text{-reduction}}$ is the potential difference between the working electrode and the reference electrode. Since the counter electrode potential increases during testing, $V_{o\text{-reduction}}$ would be smaller in the two-electrode system than that in the three-electrode system. The anodic scan can be analyzed similarly. Since the potentials of the counter electrode and the reference electrode remained the same (Fig. 5d), the $V_{o\text{-oxidation}}$ results using two- and three-electrode systems should be the same, which matches the experimental results in Fig. 5b.

According to the above experiments, the three-electrode system allows for a more accurate EW measurement due to the introduction of a reference electrode with a constant potential. However, EW measurement of electrolytes using the three-electrode system requires complex preparation processes. Meanwhile, the difference in the EW measurement results was insignificant between the two systems. Therefore, from the perspective of the practical applications of solid electrolytes in LIBs, the use of the two-electrode system for EW measurement is sufficient.

4. Conclusion

Experimental results reveal that the selection of scan mode, working electrode, and the two-electrode or three-electrode system affects EW measurement of electrolytes. Firstly, the LSV cathodic and anodic scans from the V_{oc} avoid the influence of SEI and CEI, which is the recommended scan mode. Secondly, the working electrode with a larger surface area and j_0 exhibits a smaller absolute value of overpotential and

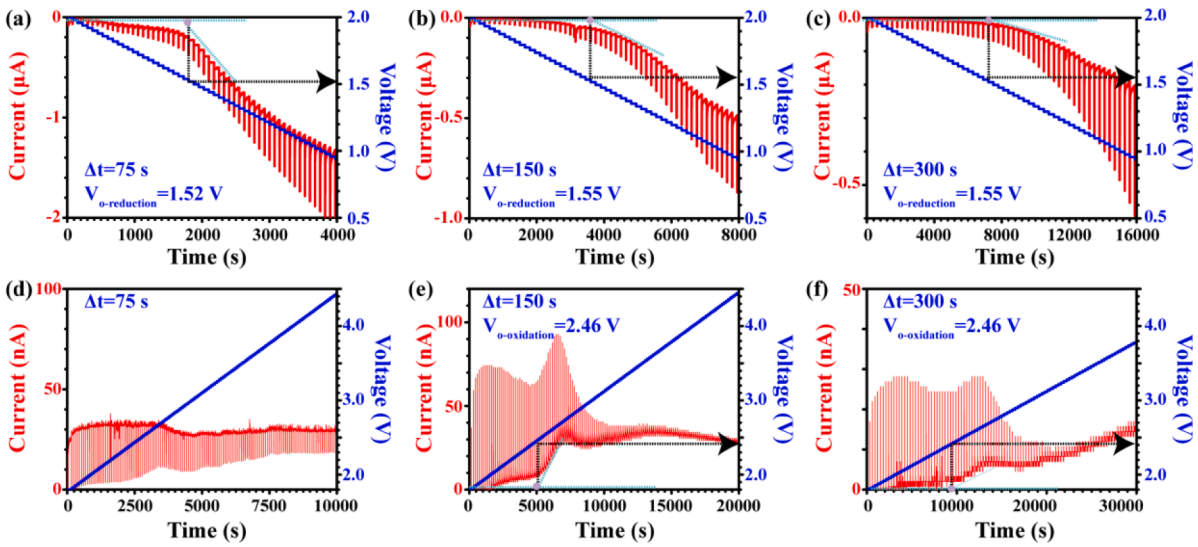

Fig. 4. SV measurement of reduction and oxidation potentials of LGPS by setting Δt at (a,d) 75 s, (b,e) 150 s, and (c,f) 300 s.

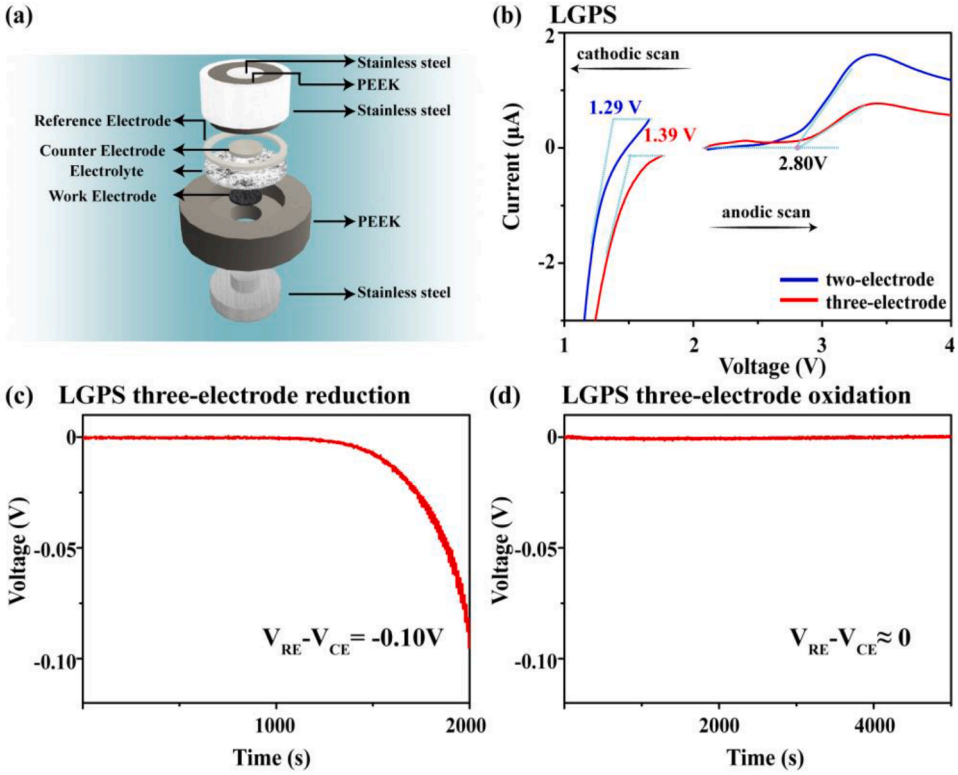

Fig. 5. (a) Schematic diagram of a three-electrode system. (b) EW measurement results of LGPS using two- and three-electrode systems. The potential difference between reference and counter electrodes during the (c) cathodic and (d) anodic scans.

the measured redox potentials are more accurate. Thirdly, the EW measurement of LGPS in the three-electrode system shows a slight increase in $V_{o\text{-reduction}}$ compared to the two-electrode system, while $V_{o\text{-oxidation}}$ results are the same in both systems.

Based on these results, the following recommendations are offered for EW measurements of electrolytes. For liquid electrolytes, it is advisable to measure EW using SS or CNT working electrodes with moderate surface areas and to perform LSV anodic and cathodic scans (scan mode 1) starting from V_{oc} to minimize the effect of SEI/CEI. For solid electrolytes, EW cannot be measured by conventional voltammetry methods using SS working electrodes with the limited surface area due to the poor interface contact, whereas the use of working electrodes with higher specific surface area results in a significant non-Faraday current, which also affects EW measurement. Therefore, the SV method using SS working electrodes is a more desirable option to improve the accuracy of the EW test with minimal non-Faraday current effect. Finally, the choice between a two- or three-electrode system can be based on specific requirements. A more accurate three-electrode system is appropriate for the investigation of the intrinsic properties of an electrolyte. For the study of electrolyte stability under real cell conditions, a two-electrode system is more practical and the preparation process is simpler.

CRediT authorship contribution statement

Zhenhan Fang: Conceptualization, Investigation, Writing – original draft. **Zixin Hong:** Conceptualization, Investigation, Writing – original draft. **Yufeng Luo:** Investigation. **Yang Liu:** Investigation. **Hengcai Wu:** Investigation. **Hui Tian:** Investigation. **Fei Zhao:** Investigation. **Yuegang Zhang:** Conceptualization, Supervision. **Qunqing Li:** Conceptualization, Supervision. **Shoushan Fan:** Conceptualization, Supervision. **Jiaping Wang:** Conceptualization, Supervision, Writing – review & editing.

Declaration of Competing Interest

The authors declare that they have no known competing financial interests or personal relationships that could have appeared to influence the work reported in this paper

Acknowledgements

This work was supported by the National Basic Research Program of China (2019YFA0705702) and the National Natural Science Foundation of China (Grant Nos. 51872158 and 51532008).

Supplementary materials

Supplementary material associated with this article can be found, in the online version, at doi:10.1016/j.electacta.2022.140210.

References

[1] L. Lu, X. Han, J. Li, J. Hua, M. Ouyang, A review on the key issues for lithium-ion battery management in electric vehicles, J. Power Sources. 226 (2013) 272–288, https://doi.org/10.1016/j.jpowsour.2012.10.060.
[2] F.T. Wagner, B. Lakshmanan, M.F. Mathias, Electrochemistry and the future of the automobile, J. Phys. Chem. Lett. 1 (2010) 2204–2219, https://doi.org/10.1021/jz100553m.
[3] D. Andre, S. Kim, P. Lamp, F. Lux, F. Maglia, Future generations of cathode materials : an automotive industry perspective, J. Mater. Chem. A 3 (2015) 6709–6732, https://doi.org/10.1039/c5ta00361j.
[4] B. Dunn, H. Kamath, J. Tarascon, Electrical energy storage for the grid : a battery of choices, Science 334 (2011) 928–936, https://doi.org/10.1126/science.1212741.
[5] Y. Ye, L.Y. Chou, Y. Liu, H. Wang, H.K. Lee, W. Huang, J. Wan, K. Liu, G. Zhou, Y. Yang, A. Yang, X. Xiao, X. Gao, D.T. Boyle, H. Chen, W. Zhang, S.C. Kim, Y. Cui, Ultralight and fire-extinguishing current collectors for high-energy and high-safety lithium-ion batteries, Nat. Energy 5 (2020) 786–793, https://doi.org/10.1038/s41560-020-00702-8.
[6] K. Wang, S. Luo, Y. Wu, X. He, F. Zhao, J. Wang, K. Jiang, S. Fan, Super-aligned carbon nanotube films as current collectors for lightweight and flexible lithium ion batteries, Adv. Funct. Mater. 23 (2013) 846–853, https://doi.org/10.1002/adfm.201202412.
[7] Z. Jin, T. Lin, H. Jia, B. Liu, Q. Zhang, L. Li, L. Zhang, Z. Su, C. Wang, Expediting the conversion of Li_2S_2 to Li_2S enables high-performance Li-S batteries, ACS Nano 15 (2021) 7318–7327, https://doi.org/10.1021/acsnano.1c00556.
[8] W. Liang, F. Lian, N. Meng, J. Lu, L. Ma, C.Z. Zhao, Q. Zhang, Adaptive formed dual-phase interface for highly durable lithium metal anode in lithium–air batteries, Energy Storage Mater. 28 (2020) 350–356, https://doi.org/10.1016/j.ensm.2020.03.022.
[9] J. Chen, X. Fan, Q. Li, H. Yang, M.R. Khoshi, Y. Xu, S. Hwang, L. Chen, X. Ji, C. Yang, H. He, C. Wang, E. Garfunkel, D. Su, O. Borodin, C. Wang, Electrolyte design for LiF-rich solid–electrolyte interfaces to enable high-performance microsized alloy anodes for batteries, Nat. Energy 5 (2020) 386–397, https://doi.org/10.1038/s41560-020-0601-1.
[10] T. Liu, S. Chen, W. Sun, L.P. Lv, F.H. Du, H. Liu, Y. Wang, Lithiophilic vertical cactus-like framework derived from Cu/Zn-based coordination polymer through *in situ* chemical etching for stable lithium metal batteries, Adv. Funct. Mater. 514 (2021) 1–12, https://doi.org/10.1002/adfm.202008514, 2008.
[11] X. Shen, R. Zhang, P. Shi, X. Chen, Q. Zhang, How does external pressure shape Li dendrites in Li metal batteries? Adv. Energy Mater. 11 (2021) 1–9, https://doi.org/10.1002/aenm.202003416.
[12] D. Cao, X. Sun, Q. Li, A. Natan, P. Xiang, H. Zhu, Lithium dendrite in all-solid-state batteries: growth mechanisms, suppression strategies, and characterizations, Matter 3 (2020) 57–94, https://doi.org/10.1016/j.matt.2020.03.015.
[13] Y. Qi, C. Ban, S.J. Harris, A New General Paradigm for Understanding and Preventing Li Metal Penetration through Solid Electrolytes, Joule 4 (2020) 2599–2608, https://doi.org/10.1016/j.joule.2020.10.009.
[14] Y. Zhu, J. Xie, A. Pei, B. Liu, Y. Wu, D. Lin, J. Li, H. Wang, H. Chen, J. Xu, A. Yang, C.L. Wu, H. Wang, W. Chen, Y. Cui, Fast lithium growth and short circuit induced by localized-temperature hotspots in lithium batteries, Nat. Commun. 10 (2019) 1–7, https://doi.org/10.1038/s41467-019-09924-1.
[15] W. Xiao, J. Wang, L. Fan, J. Zhang, X. Li, Recent advances in $Li_{1+x}Al_xTi_{2-x}(PO_4)_3$ solid-state electrolyte for safe lithium batteries, Energy Storage Mater. 19 (2019) 379–400, https://doi.org/10.1016/j.ensm.2018.10.012.
[16] Y.N. Li, C.Y. Wang, RM. Gao, F.F. Cao, H. Ye, Recent smart lithium anode configurations for high-energy lithium metal batteries, Energy Storage Mater. 38 (2021) 262–275, https://doi.org/10.1016/j.ensm.2021.03.016.
[17] M. Balaish, J.C. Gonzalez-Rosillo, K.J. Kim, Y. Zhu, Z.D. Hood, J.L.M. Rupp, Processing thin but robust electrolytes for solid-state batteries, Nat. Energy. 6 (2021) 227–239, https://doi.org/10.1038/s41560-020-00759-5.
[18] J. Sun, X. Yao, Y. Li, Q. Zhang, C. Hou, Q. Shi, H. Wang, Facilitating interfacial stability via bilayer heterostructure solid electrolyte toward high-energy, safe and adaptable lithium batteries, Adv. Energy Mater. 10 (2020) 1–11, https://doi.org/10.1002/aenm.202000709.
[19] T. Famprikis, P. Canepa, J.A. Dawson, M.S. Islam, C. Masquelier, Fundamentals of inorganic solid-state electrolytes for batteries, Nat. Mater. 18 (2019) 1278–1291, https://doi.org/10.1038/s41563-019-0431-3.
[20] Q. Zhao, S. Stalin, C.Z. Zhao, L.A. Archer, Designing solid-state electrolytes for safe, energy-dense batteries, Nat. Rev. Mater. 5 (2020) 229–252, https://doi.org/10.1038/s41578-019-0165-5.
[21] Y.S. Hu, Batteries: getting solid, Nat. Energy 1 (2016) 16042, https://doi.org/10.1038/nenergy.2016.42.
[22] Y.G. Lee, S. Fujiki, C. Jung, N. Suzuki, N. Yashiro, R. Omoda, D.S. Ko, T. Shiratsuchi, T. Sugimoto, S. Ryu, J.H. Ku, T. Watanabe, Y. Park, Y. Aihara, D. Im, I.T. Han, High-energy long-cycling all-solid-state lithium metal batteries enabled by silver–carbon composite anodes, Nat. Energy 5 (2020) 299–308, https://doi.org/10.1038/s41560-020-0575-z.
[23] L. Xu, S. Tang, Y. Cheng, K. Wang, J. Liang, C. Liu, Y.C. Cao, F. Wei, L. Mai, Interfaces in solid-state lithium batteries, Joule 2 (2018) 1991–2015, https://doi.org/10.1016/j.joule.2018.07.009.
[24] S. Ohta, T. Kobayashi, J. Seki, T. Asaoka, Electrochemical performance of an all-solid-state lithium ion battery with garnet-type oxide electrolyte, J. Power Sources. 202 (2012) 332–335, https://doi.org/10.1016/j.jpowsour.2011.10.064.
[25] L. Porz, T. Swamy, B.W. Sheldon, D. Rettenwander, T. Frömling, H.L. Thaman, S. Berendts, R. Uecker, W.C. Carter, Y.M. Chiang, Mechanism of lithium metal penetration through inorganic solid electrolytes, Adv. Energy Mater. 7 (2017) 1–12, https://doi.org/10.1002/aenm.201701003.
[26] N. Kamaya, K. Homma, Y. Yamakawa, M. Hirayama, R. Kanno, M. Yonemura, T. Kamiyama, Y. Kato, S. Hama, K. Kawamoto, A. Mitsui, A lithium superionic conductor, Nat. Mater. 10 (2011) 682–686, https://doi.org/10.1038/nmat3066.
[27] Y. Zhao, C. Wu, G. Peng, X. Chen, X. Yao, Y. Bai, F. Wu, S. Chen, X. Xu, A new solid polymer electrolyte incorporating $Li_{10}GeP_2S_{12}$ into a polyethylene oxide matrix for all-solid-state lithium batteries, J. Power Sources. 301 (2016) 47–53, https://doi.org/10.1016/j.jpowsour.2015.09.111.
[28] X.B. Cheng, R. Zhang, C.Z. Zhao, Q. Zhang, Toward safe lithium metal anode in rechargeable batteries: a review, Chem. Rev. 117 (2017) 10403–10473, https://doi.org/10.1021/acs.chemrev.7b00115.
[29] H. Duan, M. Fan, W.P. Chen, J.Y. Li, P.F. Wang, W.P. Wang, J.L. Shi, Y.X. Yin, L. J. Wan, Y.G. Guo, Extended electrochemical window of solid electrolytes via heterogeneous multilayered structure for high-voltage lithium metal batteries, Adv. Mater. 31 (2019) 1–7, https://doi.org/10.1002/adma.201807789.
[30] F. Han, Y. Zhu, X. He, Y. Mo, C. Wang, Electrochemical Stability of $Li_{10}GeP_2S_{12}$ and $Li_7La_3Zr_2O_{12}$ solid electrolytes, Adv. Energy Mater. 6 (2016) 1–9, https://doi.org/10.1002/aenm.201501590.
[31] Y. Zhu, X. He, Y. Mo, Origin of outstanding stability in the lithium solid electrolyte materials: insights from thermodynamic analyses based on first-principles calculations, ACS Appl. Mater. Interfaces 7 (2015) 23685–23693, https://doi.org/10.1021/acsami.5b07517.
[32] A. Banerjee, X. Wang, C. Fang, E.A. Wu, Y.S. Meng, Interfaces and interphases in all-solid-state batteries with inorganic solid electrolytes, Chem. Rev. 120 (2020) 6878–6933, https://doi.org/10.1021/acs.chemrev.0c00101.
[33] T. Thompson, S. Yu, L. Williams, R.D. Schmidt, R. Garcia-Mendez, J. Wolfenstine, J.L. Allen, E. Kioupakis, D.J. Siegel, J. Sakamoto, Electrochemical window of the Li-ion solid electrolyte $Li_7La_3Zr_2O_{12}$, ACS Energy Lett. 2 (2017) 462–468, https://doi.org/10.1021/acsenergylett.6b00593.
[34] X. Yu, J.B. Bates, G.E. Jellison, F.X. Hart, A stable thin-film lithium electrolyte: lithium phosphorus oxynitride, J. Electrochem. Soc. 144 (1997) 524–532, https://doi.org/10.1149/1.1837443.
[35] B. Put, P.M. Vereecken, A. Stesmans, On the chemistry and electrochemistry of LiPON breakdown, J. Mater. Chem. A (2018) 4848–4859, https://doi.org/10.1039/c7ta07928a.
[36] Y. Mo, S.P. Ong, G. Ceder, First principles study of the $Li_{10}GeP_2S_{12}$ lithium super ionic conductor material, Chem. Mater. 24 (2012) 15–17, https://doi.org/10.1021/cm203303y.
[37] A.D. Sendek, E.R. Antoniuk, E.D. Cubuk, B. Ransom, B.E. Francisco, J. Buettner-Garrett, Y. Cui, E.J. Reed, Combining superionic conduction and favorable decomposition products in the crystalline lithium-boron-sulfur system: a new mechanism for stabilizing solid Li-ion electrolytes, ACS Appl. Mater. Interfaces 12 (2020) 37957–37966, https://doi.org/10.1021/acsami.9b19091.
[38] W.D. Richards, L.J. Miara, Y. Wang, J.C. Kim, G. Ceder, Interface stability in solid-state batteries, Chem. Mater. 28 (2016) 266–273, https://doi.org/10.1021/acs.chemmater.5b04082.
[39] T. Binninger, A. Marcolongo, M. Mottet, V. Weber, T. Laino, Comparison of computational methods for the electrochemical stability window of solid-state

electrolyte materials, J. Mater. Chem. A 8 (2020) 1347–1359, https://doi.org/10.1039/c9ta09401f.
[40] Y. Xia, T. Fujieda, K. Tatsumi, P.P. Prosini, T. Sakai, Thermal and electrochemical stability of cathode materials in solid polymer electrolyte, J. Power Sources. 92 (2001) 234–243, https://doi.org/10.1016/S0378-7753(00)00533-4.
[41] Z. Fang, Y. Luo, H. Liu, Z. Hong, H. Wu, F. Zhao, P. Liu, Q. Li, S. Fan, W. Duan, J. Wang, Boosting the oxidative potential of polyethylene glycol-based polymer electrolyte to 4.36 V by spatially restricting hydroxyl groups for high-voltage flexible lithium-ion battery applications, Adv. Sci. (2021), 2100736, https://doi.org/10.1002/advs.202100736.
[42] K. Jiang, Q. Li, S. Fan, Spinning continuous carbon nanotube yarns, Nature 419 (2002) 801, https://doi.org/10.1038/419801a.
[43] P. Gao, Y. Zhu, A Course Book of Electrochemistry, Chemical Industry Press, Beijing, 2013.
[44] S. Braun, C. Yada, A. Latz, Thermodynamically consistent model for space-charge-layer formation in a solid electrolyte, J. Phys. Chem. C 119 (2015) 22281–22288, https://doi.org/10.1021/acs.jpcc.5b02679.
[45] C. Yuanxing, S. Qilei, Electrochemical Principle of Electroplating, Chemical Industry Press, Beijing, 2014.
[46] M. Egashira, H. Takahashi, S. Okada, J.I. Yamaki, Measurement of the electrochemical oxidation of organic electrolytes used in lithium batteries by microelectrode, J. Power Sources. 92 (2001) 267–271, https://doi.org/10.1016/S0378-7753(00)00553-X.
[47] Z. Anmad, Principles of Corrosion Engineering and Corrosion Control, Butterworth-Heinemann, Oxford, 2006.
[48] D. Peramunage, D.M. Pasquariello, K.M. Abraham, Polyacrylonitrile-based electrolytes with ternary solvent mixtures as plasticizers, J. Electrochem. Soc. 142 (1995) 1789–1798, https://doi.org/10.1149/1.2044195.
[49] K. Kanamura, S. Toriyama, S. Shiraishi, Z. Takehara, Studies on electrochemical oxidation of nonaqueous electrolytes using *in situ* FTIR spectroscopy, J. Electrochem. Soc. 419 (1996) 77–84, https://doi.org/10.1016/S0022-0728(96)04862-0.
[50] R.W. Schmitz, P. Murmann, R. Schmitz, R. Müller, L. Krämer, J. Kasnatscheew, P. Isken, P. Niehoff, S. Nowak, G.V. Röschenthaler, N. Ignatiev, P. Sartori, S. Passerini, M. Kunze, A. Lex-Balducci, C. Schreiner, I. Cekic-Laskovic, M. Winter, Investigations on novel electrolytes, solvents and SEI additives for use in lithium-ion batteries: systematic electrochemical characterization and detailed analysis by spectroscopic methods, Prog. Solid State Chem. 42 (2014) 65–84, https://doi.org/10.1016/j.progsolidstchem.2014.04.003.
[51] A. Méry, S. Rousselot, D. Lepage, M. Dollé, A critical review for an accurate electrochemical stability composite electrolytes, Materials 14 (2021) 3840, https://doi.org/10.3390/ma14143840 (Basel).
[52] B. Abderezzak, Introduction to Transfer Phenomena in PEM Fuel Cells, Elsevier, 2018.
[53] D. Yang, Z. Liang, C. Zhang, J.J. Biendicho, M. Botifoll, M.C. Spadaro, Q. Chen, M. Li, A. Ramon, A.O. Moghaddam, J. Llorca, J. Wang, J.R. Morante, J. Arbiol, S. L. Chou, A. Cabot, $NbSe_2$ Meets C_2N: a 2D-2D Heterostructure Catalysts as Multifunctional Polysulfide Mediator in Ultra-Long-Life Lithium–Sulfur Batteries, Adv. Energy Mater. 11 (2021), 2101250, https://doi.org/10.1002/aenm.202101250.
[54] L. Sun, M. Li, Y. Jiang, W. Kong, K. Jiang, J. Wang, S. Fan, Sulfur nanocrystals confined in carbon nanotube network as a binder-free electrode for high-performance lithium sulfur batteries, Nano Lett. 14 (2014) 4044–4049, https://doi.org/10.1021/nl501486n.
[55] X. Huang, L. Wu, Z. Huang, J. Lin, X. Xu, Characterization and testing of key electrical and electrochemical properties of lithium-ion solid electrolytes, Energy Storage Sci. Technol. 9 (2020) 479–500, https://doi.org/10.19799/j.cnki.2095-4239.2019.0296.
[56] A.V. Ivanishchev, I.A. Bobrikov, I.A. Ivanishcheva, O.Y. Ivanshina, Study of structural and electrochemical characteristics of $LiNi_{0.33}Mn_{0.33}Co_{0.33}O_2$ electrode at lithium content variation, J. Electroanal. Chem. 821 (2018) 140–151, https://doi.org/10.1016/j.jelechem.2018.01.020.
[57] A.V. Ivanishchev, A.V. Churikov, A.V. Ushakov, Lithium transport processes in electrodes on the basis of $Li_3V_2(PO_4)_3$ by constant current chronopotentiometry, cyclic voltammetry and pulse chronoamperometry, Electrochim. Acta 122 (2014) 187–196, https://doi.org/10.1016/j.electacta.2013.12.131.
[58] A.V. Ivanishchev, A.V. Ushakov, I.A. Ivanishcheva, A.V. Churikov, A.V. Mironov, S. S. Fedotov, N.R. Khasanova, E.V. Antipov, Structural and electrochemical study of fast Li diffusion in $Li_3V_2(PO_4)_3$-based electrode material, Electrochim. Acta 230 (2017) 479–491, https://doi.org/10.1016/j.electacta.2017.02.009.
[59] F. Scholz, L. Nitschke, G. Henrion, Differential staircase voltammetry-a new electroanalytical technique, Fresenius' Z. Anal. Chem. 332 (1988) 805–808, https://doi.org/10.1007/BF01129781.
[60] F. Han, T. Gao, Y. Zhu, K.J. Gaskell, C. Wang, A battery made from a single material, Adv. Mater. 27 (2015) 3473–3483, https://doi.org/10.1002/adma.201500180.